Chinese Chemical Letters 37 (2026) 111936

Contents lists available at ScienceDirect

Chinese Chemical Letters

journal homepage: www.elsevier.com/locate/cclet

Stimuli-responsive codelivery of apatinib and doxorubicin potentiates chemotherapy efficacy in breast cancer

Tingting Li[a,b,1], Yunchu Zhang[a,b,1], Siyao Che[a,b,1], Yuanyuan Zhang[a,d,1], Yin Wu[a,b], Weiling Zhuo[a,b], Xifeng Zhang[a,b], Wanyu Wang[a,b], Jiaqi Zheng[a,d], Xiang Gao[a,b], Yuzhu Hu[a,b,*], Ting Luo[a,c,*]

[a] *Department of Neurosurgery and Institute of Neurosurgery, State Key Laboratory of Biotherapy and Cancer Center, West China Hospital, West China School of Medicine, Sichuan University and Collaborative Innovation Center for Biotherapy, Chengdu 610041, China*
[b] *Department of Radiation Oncology, State Key Laboratory of Biotherapy and Cancer Center, West China Hospital, West China School of Medicine, Sichuan University and Collaborative Innovation Center for Biotherapy, Chengdu 610041, China*
[c] *Breast Disease Center, Cancer Center, West China Hospital, Sichuan University, Chengdu 610041, China*
[d] *West China School of Pharmacy, West China Hospital, Sichuan University, Chengdu 610041, China*

ARTICLE INFO

Article history:
Received 25 July 2025
Revised 24 September 2025
Accepted 7 October 2025
Available online 8 October 2025

Keywords:
Chemotherapy sensitization
Stimuli-responsive
Apatinib
Doxorubicin
Breast cancer

ABSTRACT

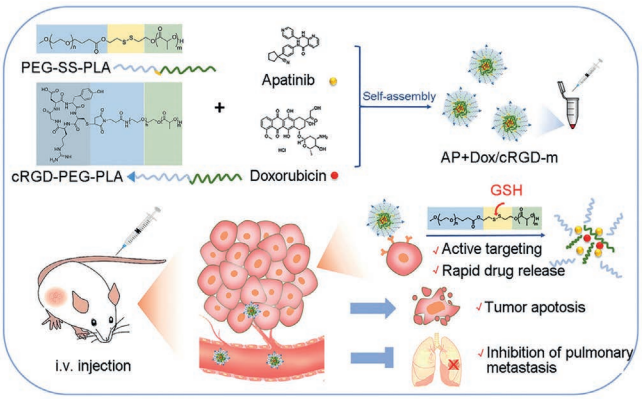
The escalating incidence of breast cancer threatens to women's health, underscoring the urgent need for the development of new therapies with reduced toxicity and increased efficacy. Combination therapy strategy holds promising potential to improve therapeutic outcomes, however, most chemotherapeutic drugs agents are hindered by poor water solubility and non-specific toxicity. The combination of chemotherapy drugs with targeted therapies represents a reliable approach. In this study, we designed a combination regimen utilizing the chemotherapeutic agent doxorubicin (Dox) alongside the anti-angiogenic drug apatinib (AP) for breast cancer treatment. Methoxy poly(ethylene glycol)-disulfide-poly(lactic acid) (PEG-SS-PLA) and cyclo(Arg-Gly-Asp-D-Tyr-Cys) conjugated PEG-PLA (cRGD-PEG-PLA) were prepared to achieve both reductive response and active targeting for co-delivery of drugs. The self-assembled drug-loaded micelles exhibited an average particle size of 61.50 nm. Our findings indicate that AP significantly enhances Dox uptake in breast cancer cells. Cellular and animal experimental results consistently demonstrated that the AP+Dox/cRGD-m effectively promotes apoptosis of breast cancer cells, while markedly inhibiting tumor growth and pulmonary metastasis. Additionally, AP+Dox/cRGD-m is biodegradable and sustainable, exhibiting a favorable safety profile *in vivo*. This study suggests that AP+Dox/cRGD-m may have potential clinical application in the treatment of breast cancer.

© 2026 Published by Elsevier B.V. on behalf of Chinese Chemical Society and Institute of Materia Medica, Chinese Academy of Medical Sciences.

Globally, breast cancer emerged as a formidable public health challenge in 2022, with 2.3 million new cases reported, representing the most frequently diagnosed malignancy and the foremost cause of cancer mortality among women [1–4]. Approximately 80% of breast cancers are aggressive and highly metastatic [5]. While chemotherapy serves as an effective treatment option, its efficacy in metastatic breast cancer is limited due to nonspecific toxicity and induced resistance [6,7]. Preclinical and clinical studies have demonstrated that combination drug therapy strategy can minimize toxicity, overcome resistance, and enhance antitumor effects by leveraging complementary drug mechanisms [8–11]. Small molecule chemotherapeutics have shown advantages in combination therapy attributed to solid research, broad range of applications, and relatively low cost [12]. Doxorubicin (Dox) is a broad-spectrum anthracycline antibiotic that inhibits DNA topoisomerase II, leading to DNA damage and apoptosis. It demonstrates significant efficacy against various malignancies, including breast cancer, hematologic malignancies, and sarcomas [13–15]. Numerous novel molecules have been developed that can modulate a variety of cancer malignancy hallmarks, including tumor invasion, metastasis, metabolism, angiogenesis, or stimulation of immune responses [16–18]. Anti-angiogenic drugs have gained particular attention, especially since vascular endothelial growth factor (VEGF) is highly expressed in early breast cancer and contributes to therapy resistance in advanced stages [19–21]. The VEGF and its receptor pathway have thus emerged as prominent therapeutic targets [22,23]. Apatinib (AP) is a VEGFR-2 inhibitor with established tolerability and efficacy, approved for advanced gastric and liver cancers [24].

* Corresponding authors.
E-mail addresses: huyuzhu023@foxmail.com (Y. Hu), luoting@wchscu.cn (T. Luo).
[1] These authors contributed equally to this work.

https://doi.org/10.1016/j.cclet.2025.111936
1001-8417/© 2026 Published by Elsevier B.V. on behalf of Chinese Chemical Society and Institute of Materia Medica, Chinese Academy of Medical Sciences.



Scheme 1. Schematic diagram illustrating the synthesis and the anti-tumor activities of AP+Dox/cRGD-m. The cRGD-functionalized nanomicelles mediate specific co-delivery of AP (a VEGFR-2 tyrosine kinase inhibitor) and Dox through integrin $\alpha v\beta 3$ binding, followed by glutathione-triggered drug release in the tumor microenvironment. This dual-action strategy simultaneously suppresses angiogenesis *via* VEGF signaling blockade and regulates cell fate through apoptosis activation and proliferation inhibition, ultimately resulting in potent inhibition of breast cancer progression and metastasis.

Studies indicate that AP combined with cisplatin more effectively inhibits tumor proliferation, migration, and invasion in MDA-MB-231 cells than either drug alone [25]. Herein, a combination regimen of AP and Dox was developed to potentiate chemotherapy (Scheme 1).

Dox is dose-limited due to severe cardiotoxicity [26–29], and both drugs exhibit hydrophobicity, resulting in non-specific diffusion and rapid clearance *in vivo* [30,31]. A nanocarrier system was engineered for the co-delivery of AP and Dox to improve blood circulation, reduce off-target toxicity and enhance drug accumulation at tumor lesions [32–35]. This nanocarrier integrates the enhanced permeability and retention (EPR) effect for passive targeting, cyclo(Arg-Gly-Asp-D-Tyr-Cys) (cRGD)-mediated active targeting [36–39] and redox-sensitive payload release, leveraging the higher intratumoral glutathione (GSH) levels (2–10 mmol/L) compared to normal tissues (1–2 μmol/L) [40–44]. Collectively, this combination strategy mitigates drug degradation, reduces toxic side effects, enhances tumor specificity, and improves the therapeutic effect.

The synthesis of reduction-responsive block polymers was validated by ^{1}H nuclear magnetic resonance (^{1}H-NMR) analysis (Figs. S1–S5 in Supporting information). The gel permeation chromatography (GPC) results of methoxy poly(ethylene glycol)-disulfide-poly(lactic acid) (PEG-SS-PLA) and maleimide (MAL)-PEG-PLA were presented (Figs. S6A and B in Supporting information). AP+Dox/cRGD-m was fabricated *via* thin film hydration technique. Dynamic light scattering (DLS) analysis revealed that the assembled AP+Dox/cRGD-m had a small particle size with a uniform distribution of 61.50 nm (Fig. S6C in Supporting information). Due to the strong reducing environment within the tumor, disulfide bonds were cleaved at elevated concentrations of GSH (2–10 mmol/L), resulting in structural disintegration to release drugs (Fig. 1A). Under normal conditions, these micelles showed uniform white spherical particles under transmission electron microscope (TEM) (Fig. 1B). The particle size of micelles maintained consistent in the absence of GSH, which exhibited a slight increase at 0.01 mmol/L GSH, while rapidly expanded at 10 mmol/L GSH (Fig. 1C). Moreover, the 10 mmol/L GSH-treated group exhibited significantly faster release of AP and Dox, along with a higher cumulative release rate within 24 h (Fig. S7 in Supporting information). TEM observation revealed irregular material sheets and fine nanoparticles, but few uniform spherical particles at 10 mmol/L GSH (Fig. 1D). These engineered nanoparticles demonstrate superior attributes compared to conventional 293 nm diameter non-responsive micelles requiring 48–96 h for drug release [45]. Dox fluorescence levels were quantitatively assessed using flow cytometric techniques. As shown in Fig. 1E, treatment with AP/m resulted in negligible signal detection. AP+Dox/m demonstrated significantly enhanced fluorescence compared to AP/m and Dox/m, and this phenomenon was especially significant in the lower concentration groups, where the red fluorescence level of the 0.2 μg/mL Dox combined with 2 μg/mL AP group had steeply increased to 59.43 % compared with 30.72 % of the equivalent concentration of the Dox. Similar findings were noted in MDA-MB-231 cells (Fig. S8 in Supporting information). Under the laser confocal microscopy (CLSM), 4T1 treated with free Dox for 2 and 7 h showed a lower red fluorescence intensity, whereas the red fluorescence intensity of Dox was increased in cells treated with AP+Dox/cRGD-m, indicating that AP improved the cellular internalization of Dox (Fig. 1F).

Dox/m exhibited dose-dependent cytotoxicity in 4T1 cells at 24 h (0.0078–2 μg/mL), whereas AP/m showed minimal effects (0.0156–4 μg/mL) (Fig. 2A). The AP+Dox/m combination demonstrated significantly enhanced cytotoxicity compared to monotherapy, particularly at Dox concentrations $\geq$1 μg/mL, with more pronounced effects after 48 h (Fig. 2B). Comparable results were observed in MDA-MB-231 cell lines (Figs. S9A and B in Supporting information). Apoptosis assessment in 4T1 cells revealed no significant effect of AP/m on apoptosis at all concentrations after 24 and 48 h, while Dox/m induced apoptosis in a concentration- and time-dependent manners (Fig. 2C, Figs. S10 and S11 in Supporting information). Notably, the AP+Dox/m group showed substantially higher apoptosis rates than single-agent groups. Consistent results were observed in the MDA-MB-231 cell line (Figs. S12 and S13 in Supporting information). Therefore, it is hypothesized that combination of AP and Dox achieves comparable cytotoxicity at lower Dox concentrations, thereby leading to reduced toxicity and improved efficacy. Western blot (WB) analyses were applied to investigate apoptosis and proliferation mechanisms. The Bcl-2-associated X protein (Bax)/B-cell lymphoma-2 (Bcl-2) ratio serves as an indicator for apoptosis, wherein Bax activation and Bcl-2 suppression synergistically trigger cytochrome c release, which subsequently initiates caspase-9 activation. The activated caspase-9 then propagates apoptotic cascade, culminating in caspase-3 activation that executes programmed cell death (Fig. 2D). Notably, the AP+Dox/m group exhibited markedly enhanced upregulation of cleaved-caspase 9 and cleaved-caspase 3 compared to monotherapies. While Dox/m and AP+Dox/m similarly affected Bax and Bcl-2, their differential activation of downstream caspases indicates intensified apoptotic signaling in the combination group (Fig. 2E). Proliferation-related protein analysis revealed that Dox/m and AP+Dox/m down-regulated phospho-extracellular regulated protein kinases (p-Erk). Additionally, AP/m, Dox/m, and AP+Dox/m significantly reduced phospho-protein kinase B (p-Akt) expression (Fig. 2F). Dox/m and AP+Dox/m also markedly reduced signal transducer and activator of transcription 3 (Stat 3) phosphorylation, whereas AP/m exhibited minimal effect, possibly because VEGF acts downstream of Stat 3 signaling pathway. Additionaly, both AP+Dox/m and Dox/m downregulates cyclin D1 and cyclin E1, effectively blocking cell cycle process, and AP+Dox/m showed no significant advantage over Dox/m, which might be due to their already low expression levels (Fig. 2F). Comparable conclusions were found in MDA-MB-231 cells (Fig. S14 in Supporting information).

The 4T1 tumor-bearing mice were allocated into six groups for systemic treatment administration through tail vein (Fig. 3A). All animal experiments were approved by the Animal Experimental Ethics Committee of State Key Laboratory of Biotherapy (SKLB), Sichuan University. Both AP/m and Dox/m groups showed certain antitumor efficacy, however, the AP+Dox/m combination therapy showed a more pronounced suppression effect compared

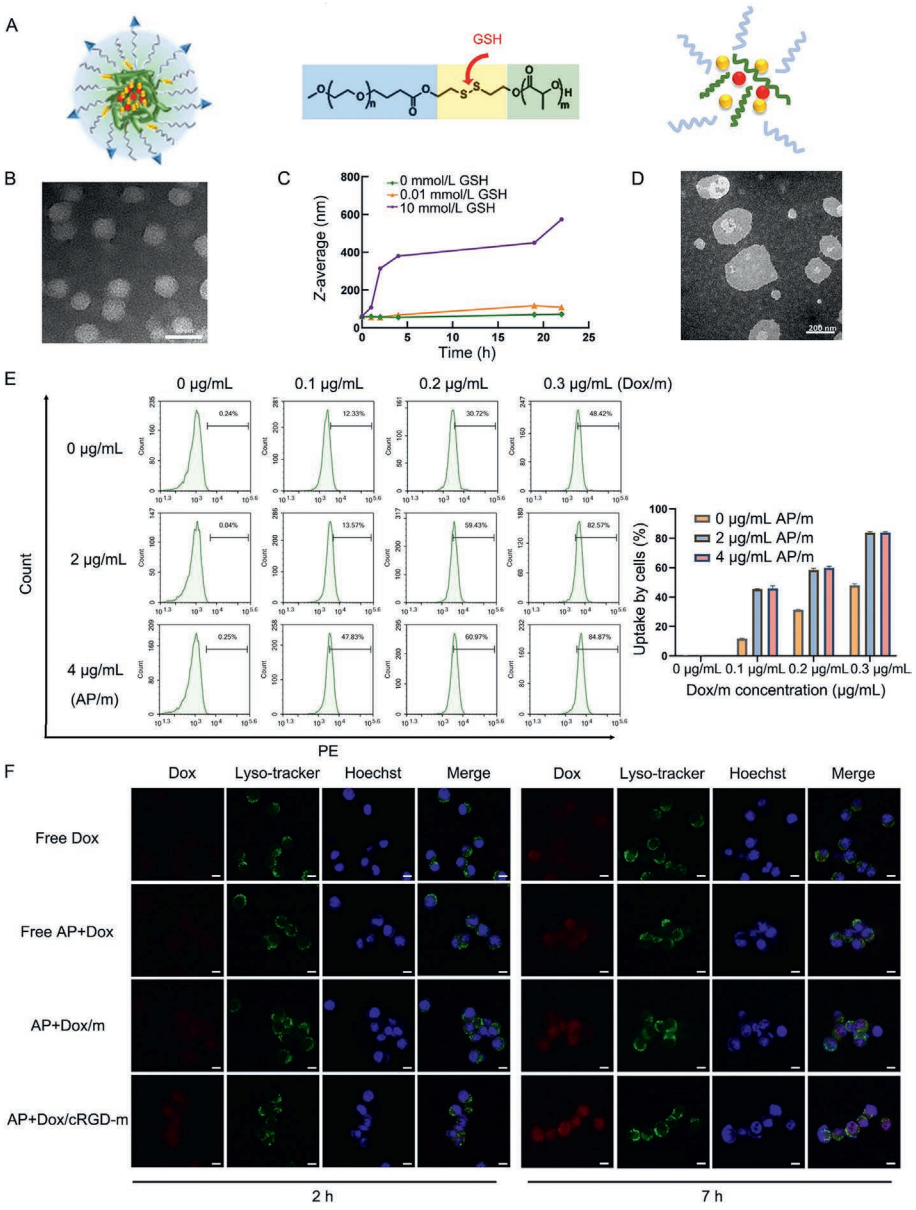


Fig. 1. Characterization and cellular uptake of nanocomposites. (A) Schematic illustration of reduction responsiveness of AP+Dox/cRGD-m. (B) TEM image of AP+Dox/cRGD-m. Scale bar: 50 nm. (C) Size distribution of micelles following treatment with varying concentrations of GSH. (D) TEM image of micelles after 24 h treatment with 10 mmol/L GSH. Scale bar: 200 nm. (E) Flow cytometry analysis depicting the uptake of Dox in 4T1 cells treated with different combinations of AP/m or Dox/m at 5 h and statistical analysis of flow cytometry data. Data are presented as mean ± standard error of the mean (SEM) ($n = 3$). (F) Confocal laser scanning microscope analysis illustrating cellular uptake of Dox by 4T1 cells after treatment with free Dox, free AP+Dox, AP+Dox/m, AP+Dox/cRGD-m for 2 and 7 h. Scale bar: 10 μm.

to monotherapy (Fig. 3B). The AP+Dox/cRGD-m showed superior tumor inhibition effect, and the tumor volume in this group was merely about 100 mm^3 (Fig. 3C). No significant body weight fluctuations occurred among treatment groups (Fig. 3D). The tumor weights of AP+Dox/cRGD-m treated group were the lowest among all treatment group (Fig. 3E). Paraffin-embedded tumor sections were stained for immunohistochemical and immunofluorescence analysis to explore the anti-tumor mechanism *in vivo*. Notably, The AP+Dox/cRGD-m group demonstrated the most substantial Ki67 index suppression relative to other experimental groups (Figs. 3F and I). The most significant reduction in the expression of CD31, a marker of vascular endothelial cells, was observed in the AP+Dox/cRGD-m group (Figs. 3G and J). The targeted combination therapy group exhibited significantly elevated terminal deoxynucleotidyl transferase mediated dUTP nick-end labeling (TUNEL)-positive cells compared to other groups (Figs. 3H and K). The results showed that AP+Dox/cRGD-m treatment significantly enhances the pro-apoptotic, anti-proliferation and anti-angiogenic effects, thereby effectively inhibiting tumor growth.

Since breast cancer is clinically prone to lung metastasis, the anti-metastatic effect of AP+Dox/cRGD-m was evaluated in a 4T1 model. A substantial number of metastatic nodules were observed in the lungs of mice in the NS and vehicle groups (Fig. 4A). Although both AP/m and Dox/m effectively suppressed lung metastasis, the AP+Dox/cRGD-m group demonstrated the fewest pulmonary nodules (Fig. 4B), with minimal lesions larger than 3 mm (Figs. 4C and D). Body weights did not differ significantly among groups (Fig. 4E). Hematoxylin-eosin (H&E) staining confirmed metastatic nodule distribution in lung sections (Fig. 4F). The findings indicate that AP+Dox/cRGD-m effectively inhibited lung metastasis than monotherapy or non-targeted combination, demonstrating promising anti-tumor and anti-metastatic efficacy

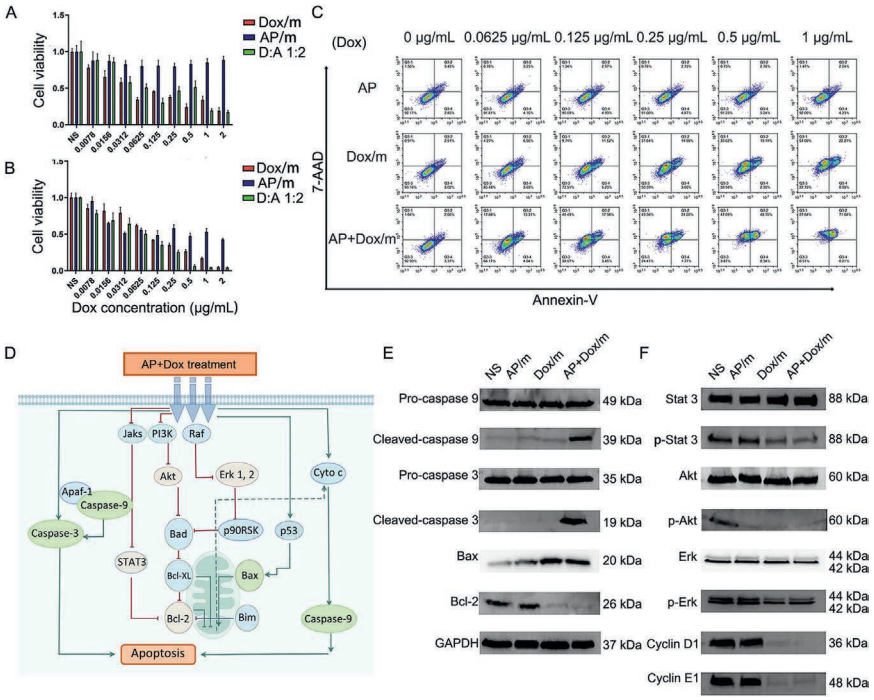


Fig. 2. Anti-tumor effect of AP/m, Dox/m and AP+Dox/m in 4T1 cell lines. (A, B) 4T1 cell viability was detected by MTT assay after treatment with different concentrations of AP/m, Dox/m and AP+Dox/m at 24 and 48 h. Data are presented as mean ± SEM ($n = 3$). (C) Cell apoptotic study in 4T1 cells. 4T1 cells treated with different concentrations of AP/m, Dox/m and AP+Dox/m for 48 h were stained by Annexin V-APC/7-AAD to analyze cell apoptosis. (D) The pathways of cell apoptosis and proliferation affected by AP+Dox/m treatment. Figure created with Figdraw. (E) WB of apoptosis-related proteins. GAPDH, glyceraldehyde-3-phosphate dehydrogenase. (F) WB of proliferation-related proteins.

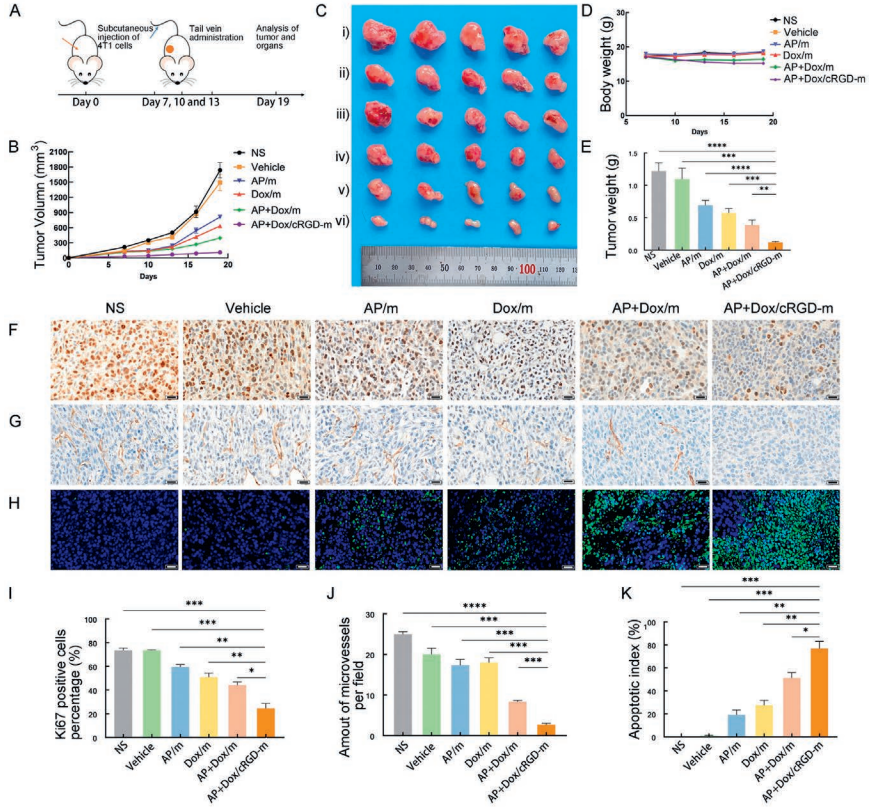


Fig. 3. Anti-tumor effects in the 4T1 subcutaneous model. (A) Treatment schedule for 4T1 subcutaneous tumor-bearing mice. (B) The tumor growth curves of 4T1 tumor-bearing mice in different treatment groups. (C) Photograph of the excised tumors from different treatments, (i) NS, (ii) Vehicle, (iii) AP/m, (iv) Dox/m, (v) AP+Dox/m, (vi) AP+Dox/cRGD-m. (D) The body weight curve of 4T1 tumor-bearing mice. (E) Tumor weight of different treatment groups ($n = 5$). (F) Ki67 staining was performed in tumor tissue sections of different groups to investigate tumor proliferation. (G) CD31 staining was applied to analyze tumor angiogenesis. (H) TUNEL staining was conducted to evaluate tumor apoptosis. Scale bar: 20 μm. (I–K) The quantitative statistical results of Ki67, CD31 and TUNEL was shown ($n = 3$). Data are presented as mean ± SEM. $^{*}P < 0.05$, $^{**}P < 0.01$, $^{***}P < 0.001$, $^{****}P < 0.0001$.

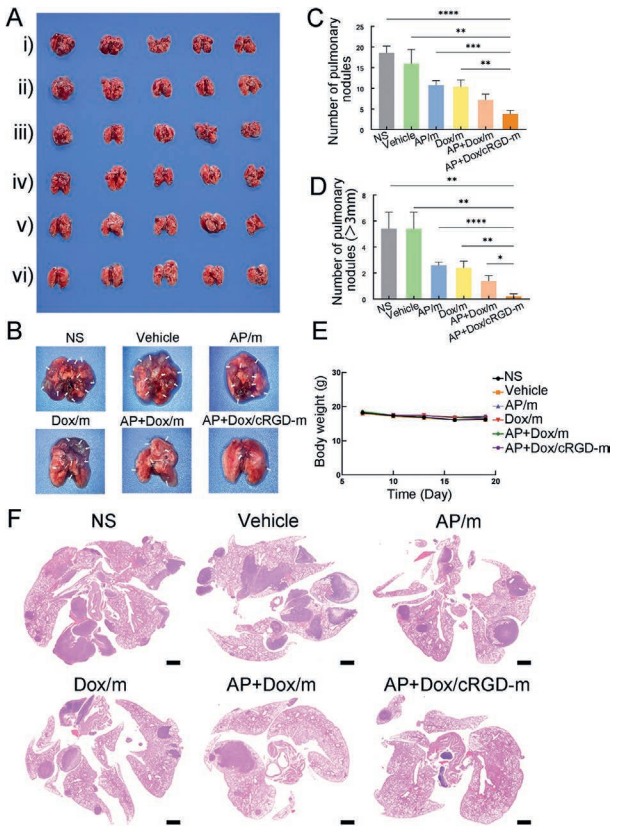


Fig. 4. Anti-tumor effects in the 4T1 pulmonary metastasis tumor model. (A) Photograph of mice lungs from different groups, (i) NS, (ii) Vehicle, (iii) AP/m, (iv) Dox/m, (v) AP+Dox/m, (vi) AP+Dox/cRGD-m. (B) Photograph of pulmonary nodules on the surface of lungs. (C) Number of pulmonary nodules. (D) Number of pulmonary nodules (>3 mm). (E) The body weight of tumor-bearing mice. (F) H&E staining of whole lungs from different treatment group. Scale bar: 1 mm. Data are presented as mean ± SEM ($n = 5$). $^{*}P < 0.05$, $^{**}P < 0.01$, $^{***}P < 0.001$, $^{****}P < 0.0001$.

against breast cancer (Fig. S15 in Supporting information). Moreover, histological examination of H&E stained vital organ sections revealed no abnormal morphological findings (Fig. S16A in Supporting information). The blood biochemical parameters across all groups suggested a favorable safety profile (Fig S16B in Supporting information). These observations suggest a potential mild myocardial inflammatory response, which may be attributable to relatively low dosage of Dox and the nanoparticle further mitigates cardiac exposure risk.

In summary, an intelligent nanocarrier with redox-responsive and active targeting capability was constructed for the co-delivery of AP and Dox. The micelles exhibited small size, high stability and reduction-sensitive drug release. AP potentiated Dox cellular internalization, and the dual-drug combination synergistically suppressed proliferation and promoted apoptosis *via* caspase activation. AP+Dox/cRGD-m significantly inhibited subcutaneous tumor growth and lung metastasis without significant toxicity. The strategy provides a feasible option for mitigating the non-specific toxicity and overcome resistance associated with Dox, offering strong clinical potential.

CRediT authorship contribution statement

Tingting Li: Writing – original draft, Project administration, Methodology, Investigation. **Yunchu Zhang:** Writing – original draft, Project administration, Methodology, Investigation, Formal analysis, Data curation. **Siyao Che:** Writing – original draft, Software, Project administration, Methodology, Investigation, Formal analysis. **Yuanyuan Zhang:** Writing – review & editing, Validation, Supervision, Investigation. **Yin Wu:** Software, Resources, Methodology, Data curation. **Weiling Zhuo:** Validation, Software. **Xifeng Zhang:** Methodology, Data curation. **Wanyu Wang:** Writing – review & editing, Software, Data curation. **Jiaqi Zheng:** Project administration, Methodology, Investigation. **Xiang Gao:** Writing – review & editing, Supervision, Resources, Funding acquisition, Conceptualization. **Yuzhu Hu:** Writing – review & editing, Supervision, Funding acquisition. **Ting Luo:** Writing – review & editing, Supervision, Resources, Funding acquisition, Conceptualization.

Declaration of competing interest

The authors declare that they have no known competing financial interests or personal relationships that could have appeared to influence the work reported in this paper.

Acknowledgments

This work was supported by the National Natural Science Foundation of China (Nos. 32222046 and 82172630), the Sichuan Science and Technology Program (No. 2023NSFSC1931), Technology innovation research and development project of Chengdu Science and Technology Bureau (No. 2024-YF05–00576-SN, China) and the 1·3·5 Project for Disciplines of Excellence, West China Hospital, Sichuan University (No. ZYYC25008). And the authors thank Dr. Shanling Wang from the Analysis and Testing Center of Sichuan University for assistance with TEM.

Supplementary materials

Supplementary material associated with this article can be found, in the online version, at doi:10.1016/j.cclet.2025.111936.

References

[1] R.L. Siegel, A.N. Giaquinto, A. Jemal, CA Cancer J. Clin. 74 (2024) 12–49.
[2] R.S. Zheng, R. Chen, B.F. Han, et al., Chin. J. Oncol. 46 (2024) 221–231.
[3] C.E. Coles, H. Earl, B.O. Anderson, et al., Lancet 403 (2024) 1895–1950.
[4] P. Gao, Y. Chen, Q. He, et al., Chin. Chem. Lett. 36 (2025) 110585.
[5] N. Harbeck, F. Penault-Llorca, J. Cortes, et al., Nat. Rev. Dis. Primers 5 (2019) 66.
[6] M.A. Harris, P. Savas, B. Virassamy, et al., Nat. Rev. Cancer 24 (2024) 554–577.
[7] B. Darvishi, M.R. Eisavand, K. Majidzadeh-A, et al., Br. J. Cancer 126 (2022) 1253–1263.
[8] C. Wang, Z. Liu, X. Chen, et al., Nat. Commun. 14 (2023) 6654.
[9] J.M. Schafer, B.D. Lehmann, P.I. Gonzalez-Ericsson, et al., Sci. Transl. Med. 12 (2020) eaaw8275.
[10] J. Huang, Y. Xu, H. Xiao, et al., ACS Nano 13 (2019) 7036–7049.
[11] H. Zhao, Z. Liu, Y. Wei, et al., ACS Nano 16 (2022) 20353–20363.
[12] P. Jaaks, E.A. Coker, D.J. Vis, et al., Nature 603 (2022) 166–173.
[13] Y. Wang, C.M. Ronckers, F.E. van Leeuwen, et al., Nat. Med. 29 (2023) 2268–2277.
[14] J. Xu, W. Zhang, Z. Cai, et al., Chin. Chem. Lett. 35 (2024) 109620.
[15] Y. Chen, L. Zeng, H. Zhu, et al., Small Methods 7 (2023) e2201086.
[16] Q. Peña, A. Wang, O. Zaremba, et al., Chem. Soc. Rev. 51 (2022) 2544–2582.
[17] Y. Zeng, F. Liu, J. Wang, et al., Chin. Chem. Lett. 36 (2025) 109734.
[18] K.C. Valkenburg, A.E. de Groot, K.J. Pienta, Nat. Rev. Clin. Oncol. 15 (2018) 366–381.
[19] M. Rusnati, G. Paiardi, C. Tobia, et al., Cancer Gene Ther. 29 (2022) 908–917.
[20] Y. Xu, J. Wang, X. Wang, et al., Cell Death Discov. 8 (2022) 36.
[21] F. Sousa, A.I. Costa-Pereira, A. Cruz, et al., J. Control. Release 339 (2021) 381–390.
[22] K. Hosaka, Y. Yang, T. Seki, et al., Nat. Commun. 11 (2020) 3704.
[23] A.S. Crystal, A.T. Shaw, L.V. Sequist, et al., Science 346 (2014) 1480–1486.
[24] H. Yao, J. Liu, C. Zhang, et al., Cell Death Dis. 12 (2021) 927.
[25] Z. Gao, M. Shi, Y. Wang, et al., Pathol. Res. Pract. 215 (2019) 152422.
[26] J. Liu, Z. Zhao, N. Qiu, et al., Nat. Commun. 12 (2021) 2425.
[27] J. Foldi, A. Silber, E. Reisenbichler, et al., npj Breast Cancer 7 (2021) 9.
[28] X. Yang, C. Huang, H. Wang, et al., ACS Nano 18 (2024) 18604–18621.
[29] W. Zhuo, W. Wang, W. Zhou, et al., Small 20 (2024) e2400630.
[30] Y. Li, Z. Cai, Z. Wang, et al., Chin. Chem. Lett. 36 (2025) 109942.
[31] Z. Lou, C. Mu, C.D. Corpstein, et al., Adv. Drug Deliv. Rev. 211 (2024) 115358.
[32] Y. Zhao, F. Fay, S. Hak, et al., Nat. Commun. 7 (2016) 11221.
[33] M. Sousa de Almeida, E. Susnik, B. Drasler, P. Taladriz-Blanco, et al., Chem. Soc. Rev. 50 (2021) 5397–5434.

[34] C. Guo, H. Yuan, Y. Wang, et al., Adv. Drug Deliv. Rev. 200 (2023) 115044.
[35] S. He, X. Gou, S. Zhang, et al., Small Methods 8 (2024) e2301127.
[36] A. Amruta, D. Iannotta, S.W. Cheetham, et al., Adv. Drug Deliv. Rev. 201 (2023) 115054.
[37] X. Liang, Y. Yang, C. Huang, et al., J. Control. Release 356 (2023) 691–701.
[38] W. Yan, B. Guo, Z. Wang, et al., J. Control. Release 360 (2023) 304–315.
[39] X. Zhu, S. Zhang, Y. Cao, et al., Chin. Chem. Lett. 34 (2023) 108234.
[40] C. Deng, Q. Zhang, J. Guo, et al., Adv. Drug Deliv. Rev. 160 (2020) 199–211.
[41] Z. Li, Y. Ma, Y. Ren, et al., J. Control. Release 362 (2023) 784–796.
[42] Y. Cheng, Y. Ji, J. Control. Release 318 (2020) 38–49.
[43] N. Krishnan, R.H. Fang, L. Zhang, Adv. Drug Deliv. Rev. 179 (2021) 114006.
[44] L.H. Fu, Y. Wan, C. Qi, et al., Adv. Mater. 33 (2021) e2006892.
[45] P. Mishra, R.K. Dey, J. Macromol. Sci. A 3 (2018) 310.